Research Article | Vol. 25, No. 17 | 21 Aug 2017 | OPTICS EXPRESS 20323
Optics EXPRESS

Real-time *in situ* study of femtosecond-laser-induced periodic structures on metals by linear and nonlinear optics

JIHUA ZHANG,[1] YIZHUO HE,[1] BILLY LAM,[1] AND CHUNLEI GUO[1,2,*]

[1]*The Institute of Optics, University of Rochester, Rochester, New York, 14627, USA*
[2]*Changchun Institute of Optics, Fine Mechanics, and Physics, Changchun 130033 China*
**chunlei.guo@rochester.edu*

Abstract: Femtosecond-laser surface structuring on metals is investigated in real time by both fundamental and second harmonic generation (SHG) signals. The onset of surface modification and its progress can be monitored by both the fundamental and SHG probes. However, the dynamics of femtosecond-laser-induced periodic surface structures (FLIPSSs) formation can only be revealed by SHG but not fundamental because of the higher sensitivity of SHG to structural geometry on metal. Our technique provides a simple and effective way to monitor the surface modification and FLIPSS formation thresholds and allows us to obtain the optimal FLIPSS for SHG enhancement.

OCIS codes: (140.3390) Laser materials processing; (140.7090) Ultrafast lasers; (240.4350) Nonlinear optics at surfaces; (240.6648) Surface dynamics.

References and links

1. A. Y. Vorobyev and C. Guo, "Direct femtosecond laser surface nano/microstructuring and its applications," Laser Photonics Rev. **7**(3), 385–407 (2013).
2. K. C. Phillips, H. H. Gandhi, E. Mazur, and S. K. Sundaram, "Ultrafast laser processing of materials: a review," Adv. Opt. Photonics **7**(4), 684–712 (2015).
3. D. W. Bäuerle, *Laser Processing and Chemistry* (Springer Science & Business Media, 2013).
4. E. Kannatey-Asibu, Jr., *Principles of Laser Materials Processing* (John Wiley & Sons, 2009).
5. R. Fang, A. Vorobyev, and C. Guo, "Direct visualization of the complete evolution of femtosecond laser-induced surface structural dynamics of metals," Light Sci. Appl. **6**(3), e16256 (2017).
6. M. Birnbaum, "Semiconductor surface damage produced by ruby lasers," J. Appl. Phys. **36**(11), 3688–3689 (1965).
7. Z. Guosheng, P. M. Fauchet, and A. E. Siegman, "Growth of spontaneous periodic surface structures on solids during laser illumination," Phys. Rev. B **26**(10), 5366–5381 (1982).
8. J. F. Young, J. E. Sipe, and H. M. van Driel, "Laser-induced periodic surface structure. III. Fluence regimes, the role of feedback, and details of the induced topography in germanium," Phys. Rev. B **30**(4), 2001–2015 (1984).
9. J. Bonse, S. Höhm, S. V. Kirner, A. Rosenfeld, and J. Krüger, "Laser-induced periodic surface structures - a scientific evergreen," IEEE J. Sel. Top. Quant. **23**(3), 1–15 (2017).
10. J. Bonse, J. Krüger, S. Höhm, and A. Rosenfeld, "Femtosecond laser-induced periodic surface structures," J. Laser Appl. **24**(4), 042006 (2012).
11. J. Bonse, S. Baudach, J. Krüger, W. Kautek, and M. Lenzner, "Femtosecond laser ablation of silicon–modification thresholds and morphology," Appl. Phys., A Mater. Sci. Process. **74**(1), 19–25 (2002).
12. A. Borowiec and H. K. Haugen, "Subwavelength ripple formation on the surfaces of compound semiconductors irradiated with femtosecond laser pulses," Appl. Phys. Lett. **82**(25), 4462–4464 (2003).
13. M. Y. Shen, C. H. Crouch, J. E. Carey, R. Younkin, E. Mazur, M. Sheehy, and C. M. Friend, "Formation of regular arrays of silicon microspikes by femtosecond laser irradiation through a mask," Appl. Phys. Lett. **82**(11), 1715–1717 (2003).
14. Y. Shimotsuma, P. G. Kazansky, J. Qiu, and K. Hirao, "Self-organized nanogratings in glass irradiated by ultrashort light pulses," Phys. Rev. Lett. **91**(24), 247405 (2003).
15. Q. Wu, Y. Ma, R. Fang, Y. Liao, Q. Yu, X. Chen, and K. Wang, "Femtosecond laser-induced periodic surface structure on diamond film," Appl. Phys. Lett. **82**(11), 1703–1705 (2003).
16. T. Q. Jia, H. X. Chen, M. Huang, F. L. Zhao, J. R. Qiu, R. X. Li, Z. Z. Xu, X. K. He, J. Zhang, and H. Kuroda, "Formation of nanogratings on the surface of a ZnSe crystal irradiated by femtosecond laser pulses," Phys. Rev. B **72**(12), 125429 (2005).
17. S. K. Das, D. Dufft, A. Rosenfeld, J. Bonse, M. Bock, and R. Grunwald, "Femtosecond-laser-induced quasiperiodic nanostructures on TiO2 surfaces," J. Appl. Phys. **105**(8), 084912 (2009).

#301419 https://doi.org/10.1364/OE.25.020323
Journal © 2017 Received 30 Jun 2017; revised 6 Aug 2017; accepted 7 Aug 2017; published 11 Aug 2017

Optics EXPRESS

18. D. Dufft, A. Rosenfeld, S. K. Das, R. Grunwald, and J. Bonse, "Femtosecond laser-induced periodic surface structures revisited: A comparative study on ZnO," J. Appl. Phys. **105**(3), 034908 (2009).
19. J. Wang and C. Guo, "Formation of extraordinarily uniform periodic structures on metals induced by femtosecond laser pulses," J. Appl. Phys. **100**(2), 023511 (2006).
20. A. Y. Vorobyev and C. Guo, "Femtosecond laser-induced periodic surface structure formation on tungsten," J. Appl. Phys. **104**(6), 063523 (2008).
21. T. Y. Hwang and C. Guo, "Angular effects of nanostructure-covered femtosecond laser induced periodic surface structures on metals," J. Appl. Phys. **108**(7), 073523 (2010).
22. A. Y. Vorobyev and C. Guo, "Metallic light absorbers produced by femtosecond laser pulses," Adv. Mech. Eng. **2**, 452749 (2010).
23. G. Miyaji, W. Kobayashi, and K. Miyazaki, "Femtosecond-laser-induced nanostructure formation and surface modification of diamond-like carbon film," Electrochim. Acta **53**(1), 167–170 (2007).
24. S. Höhm, A. Rosenfeld, J. Krüger, and J. Bonse, "Femtosecond diffraction dynamics of laser-induced periodic surface structures on fused silica," Appl. Phys. Lett. **102**(5), 054102 (2013).
25. X. D. Guo, R. X. Li, Y. Hang, Z. Z. Xu, B. K. Yu, H. L. Ma, B. Lu, and X. W. Sun, "Femtosecond laser-induced periodic surface structure on ZnO," Mater. Lett. **62**(12), 1769–1771 (2008).
26. G. S. Agarwal and S. S. Jha, "Surface-enhanced second-harmonic generation at a metallic grating," Phys. Rev. B **26**(2), 482–496 (1982).
27. G. A. Farias and A. A. Maradudin, "Second-harmonic generation in reflection from a metallic grating," Phys. Rev. B **30**(6), 3002–3015 (1984).
28. J. L. Coutaz, M. Neviere, E. Pic, and R. Reinisch, "Experimental study of surface-enhanced second-harmonic generation on silver gratings," Phys. Rev. B Condens. Matter **32**(4), 2227–2232 (1985).
29. M. Nevière, R. Reinisch, and D. Maystre, "Surface-enhanced second-harmonic generation at a silver grating: A numerical study," Phys. Rev. B Condens. Matter **32**(6), 3634–3641 (1985).
30. R. Reinisch, M. Neviere, H. Akhouayri, J. L. Coutaz, D. Maystre, and E. Pic, "Grating enhanced second harmonic generation through electromagnetic resonances," Opt. Eng. **27**(11), 271161 (1988).
31. K. Liu, L. Zhan, Z. Y. Fan, M. Y. Quan, S. Y. Luo, and Y. X. Xia, "Enhancement of second-harmonic generation with phase-matching on periodic sub-wavelength structured metal film," Opt. Commun. **276**(1), 8–13 (2007).
32. P. Genevet, J. P. Tetienne, E. Gatzogiannis, R. Blanchard, M. A. Kats, M. O. Scully, and F. Capasso, "Large enhancement of nonlinear optical phenomena by plasmonic nanocavity gratings," Nano Lett. **10**(12), 4880–4883 (2010).
33. J. Renger, R. Quidant, N. van Hulst, and L. Novotny, "Surface-enhanced nonlinear four-wave mixing," Phys. Rev. Lett. **104**(4), 046803 (2010).
34. Y. Ogata and C. Guo, "Nonlinear optics on nano/micro-hierarchical structures on metals: focus on symmetric and plasmonic effects," Nano Rev. Experiments **8**(1), 1339545 (2017).
35. A. Y. Vorobyev and C. Guo, "Enhanced absorptance of gold following multipulse femtosecond laser ablation," Phys. Rev. B **72**(19), 195422 (2005).
36. A. Y. Vorobyev and C. Guo, "Reflection of femtosecond laser light in multipulse ablation of metals," J. Appl. Phys. **110**(4), 043102 (2011).
37. M. Huang, F. Zhao, Y. Cheng, N. Xu, and Z. Xu, "Origin of Laser-Induced Near-Subwavelength Ripples: Interference between Surface Plasmons and Incident Laser," ACS Nano **3**(12), 4062–4070 (2009).

1. Introduction

Laser-matter interaction has been extensively investigated ever since the invention of laser in 1960. High-intensity lasers are able to directly melt, ablate and alter material surfaces of a wide range of materials including metals, semiconductors, dielectrics and organics. Ultrafast laser processing of materials, in particular, benefits from numerous advantages over other types and enables a broad range of interesting applications [1, 2]. In laser processing, understanding the physical mechanism and revealing the dynamic process of the laser-surface interaction are highly important to control and produce desired surface structures for specific applications. A significant amount of both theoretical and experimental research efforts have been invested in this topic [3–5].

One interesting surface-structure phenomenon following laser irradiation is the formation of laser-induced periodic surface structures (LIPSSs), which is attributed to the interference between the incident laser and the excited surface plasmons on the surface [6–9]. LIPSS have been produced on a variety of materials including semiconductors, metals, and dielectrics in the past. More recently, femtosecond-laser-induced periodic surface structures (FLIPSSs) have been extensively studied due to their ability to modify the optical, chemical, physical and wetting properties of various materials [1, 10]. FLIPSS were first produced on

Optics EXPRESS

semiconductors and dielectrics by others [11–18] and on metals by us [19–22]. Linear optical signals have been used to study the FLIPSS formation dynamics with pulse number on carbon film and fused silica [23, 24]. Nonlinear second harmonic generation (SHG) has also been applied to explain the mechanism of high spatial frequency FLIPSS and the resultant SHG enhancement was reported on ZnO [18, 25]. As widely reported, regular metal grating can enhance nonlinear optics such as SHG [26–31] and four wave mixing (FWM) [32, 33] due to the plasmonic resonances. Recently, we reported that FLIPSS on metal can also modify the surface SHG property significantly [34]. Surprisingly however, to our knowledge SHG has never been used to probe the FLIPSS formation on metal in spite of its high sensitivity on said structures.

In this work, we investigated both the fundamental frequency (FF) and nonlinear SHG dynamics reflected from a metal surface during the femtosecond (fs)-laser processing as a function of the pulse number and the incident fluence. A single beam is applied to induce both the ablation and the detected reflection signals at the same time. This setup ensures the real-time and *in situ* monitoring of surface modification. As the result, a clear correlation is established between the intensity of the reflected signals and the surface morphology. Especially, the FLIPSS formation on metal surface is revealed by the nonlinear reflection by an increase during the first hundreds of pulses. The reflection dynamics are further discussed by comparing with the surface morphology induced by different pulse numbers. Our proposal paves a simple and new way to study the fs-laser-induced surface structure change in real time and to realize surface structures optimized for antireflection or nonlinear optics.

2. Experiment

Figure 1 shows the schematic of the experimental setup. A beam from a Ti: Sapphire fs laser (65-fs pulses at 1 kHz with center wavelength of 800 nm) is focused by a lens with focal length of 300 mm onto the polished copper surface. The incident angle θ is 45° and *p* polarization is utilized for the ablation. A long-pass filter (FGL665M) is used to eliminate the second harmonic wavelength from the laser source. The real-time reflection beam which includes both the FF and SHG is collected by another lens and then detected by a photomultiplier tube (PMT) after beam selection by filters. In the FF measurement, the setup is shown in the dashed box. The FF is selected by a long-pass filter (FGL665M). A neutral density filter is used to attenuate the FF beam power into the PMT. The setup for the SHG measurement is shown in the dash-dotted box. The SHG is selected by a combination of a short-pass filter (FGB39) and a band-pass filter (FGB37M). The signal from the PMT is read out by a lock-in amplifier. An electrical shutter is utilized to control the number of laser pulses. The sample surface morphologies after different pulse numbers were characterized using a 3D laser scanning microscope (VK-9700) and a scanning electron microscopy (SEM) (Hitachi S-4100).

In fs-laser processing, the surface temperature rise and structure change take place after the pulse [2]. Clearly, if we measure the linear FF and nonlinear SHG reflections excited by the same fs-laser beam used for ablation, they are generated before the surface change due to the instantaneous response. Therefore, the collected signals in our experiments are determined by (and thus are able to reflect) the surface morphology after previous laser pulses.

3. Results and discussion

In the first step, we applied the SHG setup and measured the signal reflected from a polished surface at FF fluences below the ablation threshold. Figure 2 shows the fluence dependence of the collected signals (solid black squares) and a quadratic relationship line (solid red line). The quadratic relation between the signal intensity and the FF fluence is clear before 7 mJ/cm^2, which verifies the SHG signal.

Optics EXPRESS

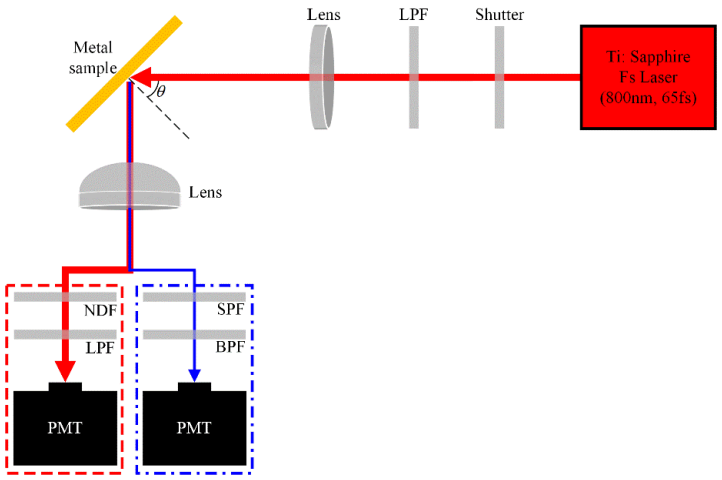

Fig. 1. Schematic of the experimental setup. The setups in the dashed and dash-dotted boxes are used in the FF and SHG measurement, respectively. LPF: long-pass filter, SPF: short-pass filter, BPF: band-pass filter, NDF: neutral density filter, PMT: photomultiplier tube.

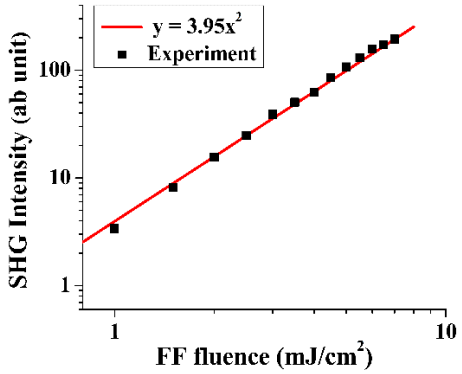

Fig. 2. SHG intensity as a function of the FF fluence lower than the ablation threshold. The solid line is a quadratic relationship line.

After verification of SHG, the real-time reflected FF and SHG as a function of the pulse number were measured in the ablation process for three laser fluences. Figures 3(a)-3(c) and 3(d)-3(f) show the FF and SHG results, respectively. Figures 3(g), 3(h) and 3(i) are the corresponding surface morphologies after 500 pulses for three fluences. In the experiment, all measurements were repeated five times for the linear case and ten times for the nonlinear case, from which the mean value and the standard error bar were obtained. The main experimental error, especially the first effective data point at 50 pulses, comes from the data-averaging effect of the lock-in amplifier and the uncontrolled time delay between the time to open the shutter and the time to collect the first effective data point. In the lock-in amplifier, every data is an averaged output over the last 5 time constants, which is 50 milliseconds in our case. If the time delay is Δt milliseconds, the first effective data point would be the average over Δt milliseconds after and 50-Δt milliseconds before opening the shutter. While the signal before opening the shutter is just noise and very weak. Other mechanisms contributing to the error bar include tilt of the sample surface and fluctuation of the laser output power.

For the FF reflection with a fluence of 5.5 mJ/cm^2, the signal remains constant after the initial rise. This means the fluence is below the ablation threshold and no surface structure modification occurs in the laser processing, as verified by the surface morphology after 500 pulses in Fig. 3(g). Note that the holes and particles are originally on the surface before laser

Optics EXPRESS

irradiation. As power exceeds the ablation threshold, which is the case in Figs. 3(b) and 3(c), the reflected FF signal decreases from the beginning. This reflection reduction is due to the high intensity of laser and the laser-induced surface structures, as shown in Figs. 3(h) and 3(i). Detailed analysis and mechanisms of absorption/reflection dynamics have been discussed in [35, 36]. For the fluence of 65.9 mJ/cm^2, some microscale structures are formed after 500 pulses. For higher fluence of 175.5 mJ/cm^2, the reflection reduction speed is faster, which means faster surface modification. From the SEM image in Fig. 3(i), the FLIPSS show up at this fluence level.

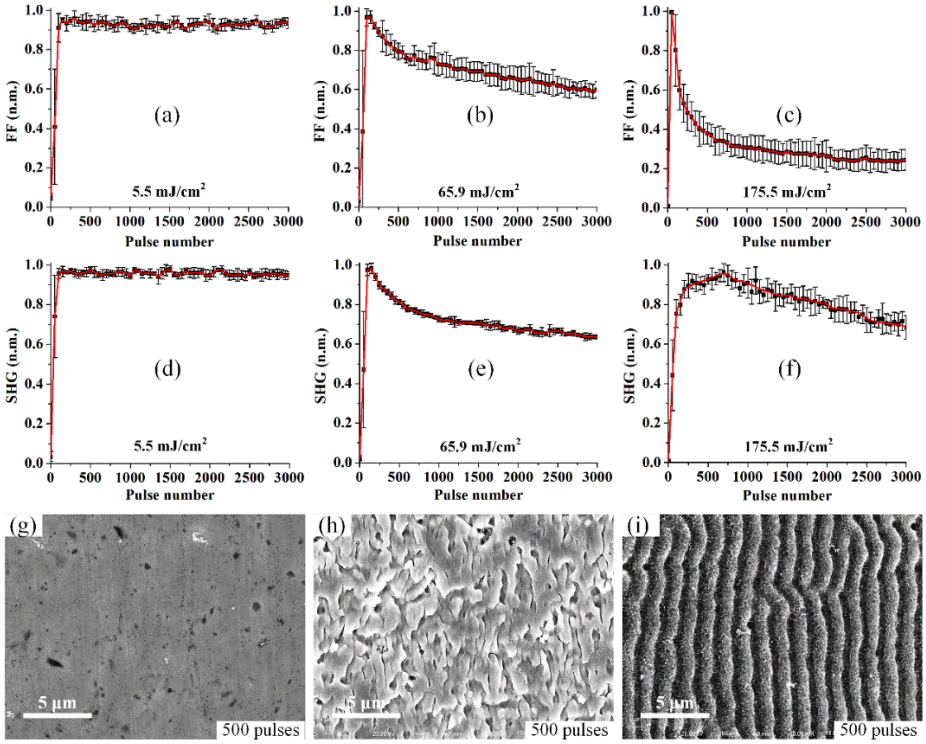

Fig. 3. Real-time measurement of reflected (a, b, c) FF and (d, e, f) SHG signals in the laser ablation process when the irradiated laser fluence is (a, d) 5.5 mJ/cm^2, (b, e) 65.9 mJ/cm^2 and (c, f) 175.5 mJ/cm^2. (g), (h) and (i) are the corresponding surface morphologies after 500 pulses for three fluences. The experiment data are normalized.

By monitoring the real time linear reflection, we can tell the occurrence of ablation and the ablation speed. It is also a simple way to obtain the ablation threshold by monitoring the onset of the reflection decrease. For example, the ablation threshold is found to be 11 mJ/cm^2 in our case. However, as in our previous work in [36], the linear reflection is unable to provide any indication if FLIPSS are formed or not. This is because the influence of FLIPSS on the linear reflection makes small difference to other formed surface structures. Conversely, we've observed SHG to be very sensitive to FLIPSS in our previous study [34]. In order to reveal the FLIPSS formation, we then monitored the real-time reflected SHG.

Figure 3(d) shows the SHG dynamics with pulse number when the fluence is below the ablation threshold. It also remains constant after the initial rise. This is expected as the surface property is not changed. When the fluence increases to 65.9 mJ/cm^2 in Fig. 3(e), the SHG decreases with pulse numbers after the initial rise, which is similar to the linear reflection. The primary cause of the SHG drop is the enhanced absorption of FF and SHG by the laser-induced surface structures and the generation of a crater. With the fluence continually increasing to 175.5 mJ/cm^2, an interesting phenomenon occurs. The variation of the real-time

Optics EXPRESS

SHG with pulse number shows a new trend. As shown in Fig. 3(f), after laser irradiation, the SHG firstly undergoes a quick increase with laser pulses. After 200 pulses, the SHG continues to increase, but at a slower rate. At a specific pulse number around 700, the SHG reaches its maximum and then drops slowly.

In order to have a better understanding of the SHG dynamics at this fluence, we irradiate the sample with different pulse numbers and plot the detailed surface structures in Fig. 4 and the crater profiles in Fig. 5. Based on the structures resulting from different pulse numbers, we can see that the FLIPSS begin to form at fluence larger than the FLIPSS threshold. The clear FLIPSS formation starts at around 200 pulses. As shown in Fig. 4(e), the first created quasi-periodic structures connect to each other and regular FLIPSS are formed. In this process, the metal surface is relatively flat compared with the wavelength. Thus, the SHG reflection is mainly determined by the surface structures. As studied before, FLIPSS can increase the SHG signal significantly due to the plasmonic field enhancement. Therefore, the

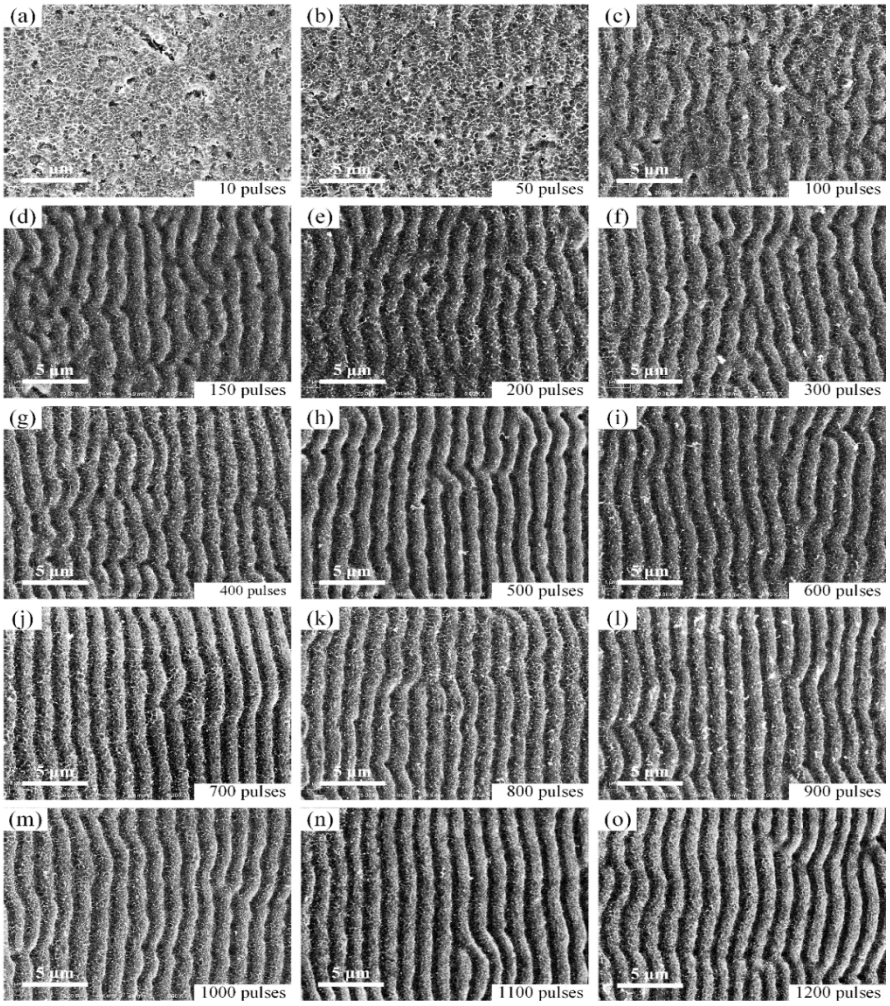

Fig. 4. Surface structures after different pulse numbers when the laser fluence is 175.5 mJ/cm^2

Optics EXPRESS

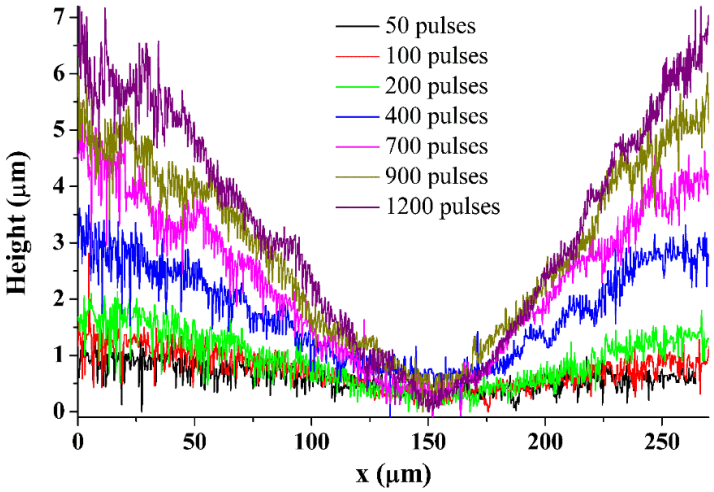

Fig. 5. Height profiles of craters after different pulse numbers for 175.5 mJ/cm^2.

SHG reflection increases quickly. With the number of pulses increasing, on the one hand, the area of the extended FLIPSS formation becomes larger and the depth of the FLIPSS becomes deeper [37]. The combined contribution of these structure changes further enhance the SHG. On the other hand, as shown in Fig. 5, a crater is formed after 200 pulses and becomes deeper and deeper. The formation of craters can lower the SHG reflection and counteract part of the SHG enhancement by the FLIPSS, which reduces the slope of SHG rise. After a specific pulse number, the SHG reduction due to cratering surpasses the enhancement by the FLIPSS. At this point, the SHG signal begins to decrease with pulse number.

Other mechanisms may also play a role in this process. First, the area of the extended FLIPSS formation decreases after a certain pulse number due to the increased re-deposition above and below the FLIPSS area or the disappearance of FLIPSS in the center area with high local fluence. Secondly, an interesting phenomenon of grating-enhanced SHG on metal predicted by theory [29, 30] and demonstrated by experiment [28] lies in the existence of an optimized grating depth for realizing maximum SHG enhancement. The change of FLIPSS depth with pulse number can also make a change to the SHG. Other contributions include the diffraction to higher orders with increasing the FLIPSS depth and the surface structure caused transition from the specular reflection to the diffuse one [36]. As part of the higher-order diffraction and diffuse reflection may not be able to be collected by the PMT.

It is worth noting that in the experiment, a Gauss beam is utilized and the incident angle is 45°. As a result, the local fluence in the beam cross section is not uniform on the metal surface. This causes the FLIPSS have different local properties at different locations as both the FLIPSS period and depth are related to laser fluence. The non-uniformity of the FLIPSS makes the SHG an average effect in the beam cross section. Even still, our result clearly shows that the FLIPSS formation is responsible for the disparate SHG dynamics in Fig. 3(f). Correspondingly, the real-time *in situ* SHG measurement is a simple and effective technique for probing the FLIPSS formation.

To further verify the proposed method, we also studied the correlation between SHG and FLIPSS at different fluence levels. Figure 6(a) shows the SHG dynamics for four different fluences of 175.5 mJ/cm^2, 197.5 mJ/cm^2, 219.5 mJ/cm^2 and 241.5 mJ/cm^2. Here we only give the normalized mean values based on 10 times of measurements at every fluence. Similar dynamics are visualized for different fluences. For example, the rise slope change, where the crater effect comes into play, occurs at 200, 200, 150 and 100 pulses and the maximum SHG occurs at 700, 550, 500 and 350 pulses for the fluences of 175.5 mJ/cm^2, 197.5 mJ/cm^2,

Optics EXPRESS

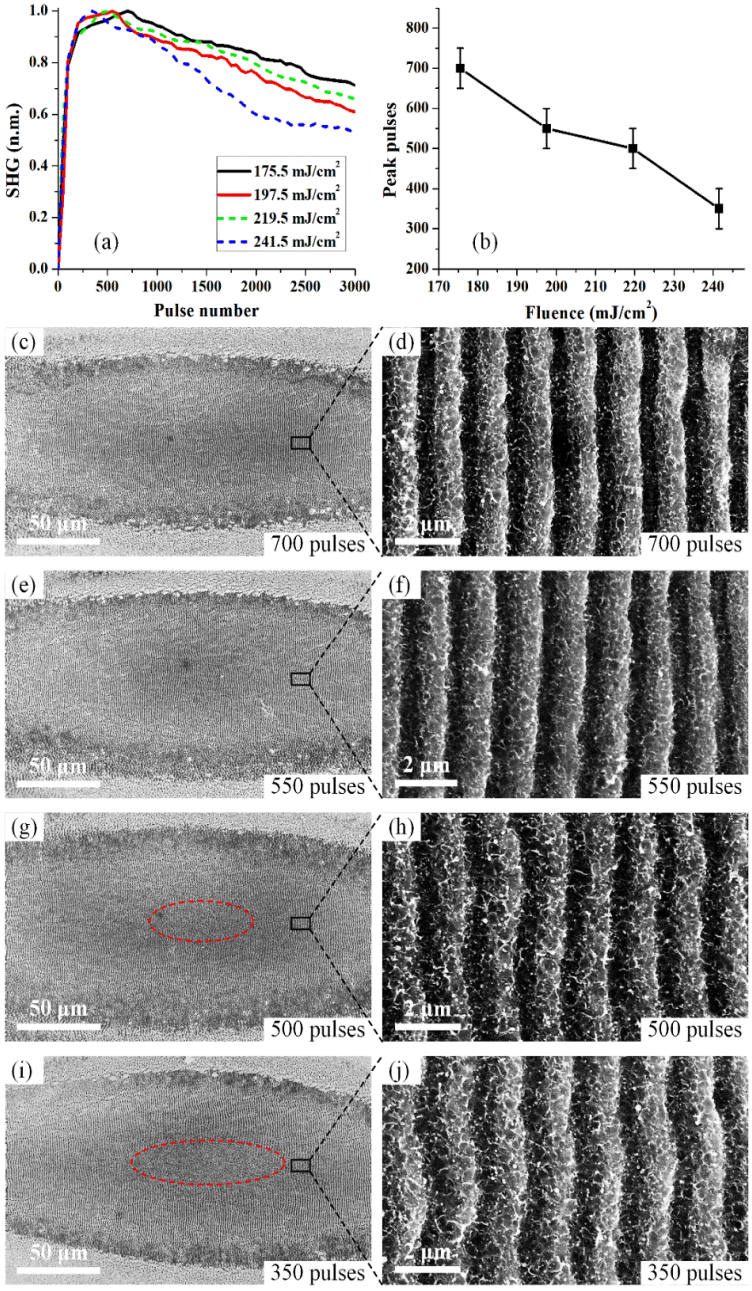

Fig. 6. (a) Normalized SHG signal as a function of the pulse number for different laser fluences. (b) Peak pulse number as a function of the laser fluence. Surface structures and enlarged views of FLIPSS after (c, d) 700 pulses for 175.5 J/cm^2, (e, f) 550 pulses for 197.5 mJ/cm^2, (g, h) 500 pulses for 219.5 mJ/cm^2 and (i, j) 350 pulses for 241.5 mJ/cm^2. Solid rectangles in (c), (e), (g) and (i) indicate the position of the enlarged FLIPSS. Dashed ellipses in (g) and (i) mark out the areas where FLIPSS are disappeared.

219.5 mJ/cm^2 and 241.5 mJ/cm^2, respectively. Figures 6(c), 6(e), 6(g) and 6(i) show the surface morphologies in the beam cross section after 700 pulses for 175.5 mJ/cm^2, 550 pulses for 197.5 mJ/cm^2, 500 pulses for 219.5 mJ/cm^2 and 350 pulses for 241.5 mJ/cm^2, respectively. Figures 6(d), 6(f), 6(h) and 6(j) are the corresponding enlarged views of

Optics EXPRESS

FLIPSS. We can see that after the peak pulse, all the fluences result in good FLIPSS formation, which is responsible for the SHG rise before the peak pulses.

However, the rise and fall of SHG are not always faster for higher fluences as we expected, such as the comparison between 197.5 mJ/cm^2 and 219.5 mJ/cm^2. Indeed, we found two sets of fluences that result in different surface structures. For the fluences of 175.5 J/cm^2 and 197.5 mJ/cm^2, large area of FLIPSS (~220 μm × 80 μm) is fabricated within the beam spot after peak pulses. The FLIPSS are clean and regular, as shown in Figs. 6(d) and 6(f). With respect to higher fluences of 219.5 J/cm^2 and 241.5 mJ/cm^2, more nanostructures are covered on the FLIPSS after peak pulses. As marked out in Figs. 5(g) and 5(i) by the red dashed ellipses, the center area of the FLIPSS is disappeared because the laser parameter in this area is beyond the specific FLIPSS condition at these two high fluences. This also explains why the increase and decrease speeds are faster at 197.5 mJ/cm^2 than at 219.5 mJ/cm^2 even with lower fluence. Because the FLIPSS area is smaller at 219.5 mJ/cm^2. Therefore, the SHG dynamics can also provide useful information for fabricating large area and clean FLIPSS. The FLIPSS period and depth at optimized pulses are also different with fluences. The period is larger for higher fluence, which are 1.359 μm, 1.456 μm, 1.495 μm and 1.522 μm in Figs. 6(d), 6(f), 6(h) and 6(j), respectively. The dependence of the period on fluence is consistent with previous works [4]. According to the laser-scanning microscope measurement, the corresponding depths are 640 nm, 560 nm, 490 nm and 400 nm, respectively.

Based on the above results, the FLIPSS formation process is clearly revealed by the nonlinear dynamics with a first increase followed by a decrease, which is absent in the linear-reflection measurement. This essentially is a dynamic monitoring of the FLIPSS formation and is very useful in fabricating FLIPSS and in producing various functionalized surfaces with FLIPSS. This technique provides us with a way to obtain the optimized pulse number for fabricating FLIPSS with the highest SHG efficiency and without significant cratering. Furthermore, it also monitors the ablation and FLIPSS formation thresholds by the onset of direct decrease and an increase before decreasing, respectively. For example, the ablation and FLIPSS thresholds are found to be 11 mJ/cm^2 and 143 mJ/cm^2 respectively based on the SHG dynamics. In practice, this technique can be simply implemented by monitoring the reflected SHG as a function of time (pulse numbers) while increasing the fluence until the increase trend is observed after the initial rise. Based on this technique, we fabricated high-quality FLIPSS on other metals in addition to copper studied here. For example, after the fluence increased to 252.8 mJ/cm^2, we observed the SHG increase and peak after 550 pulses on silver. Correspondingly, good FLIPSS are realized in the beam cross section based on the related laser parameters.

4. Conclusion

In conclusion, the fs-laser-induced surface morphology modification and FLIPSS formation process are revealed by the same beam excited linear and nonlinear reflection in real time. This simple method not only provides a way to obtain the ablation/FLIPSS thresholds for a specific material, but also gives a clue on the ablation speed and surface relief dynamics with pulse numbers. In particular, the collected SHG signal shows a distinct increase before decreasing when the laser fluence exceeds the FLIPSS threshold. This phenomenon is absent in the linear reflection. The proposed real-time monitoring with single beam paves a new way to realize surface morphology optimized for SHG enhancement, and can be readily applied to realize other expected surface functions on different materials. The optimal surface structures for SHG enhancement can enable a range of SHG-related studies, such as molecular detection, biological sensing, and chemical applications.

Funding

US Army Research Office; Bill & Melinda Gates Foundation; Boeing; AlchLight.